A Fail-Safe Semi-Centralized Impedance Controller: Validation on a Parallel Kinematics Ankle

Francesco Ruscelli, Arturo Laurenzi, Enrico Mingo Hoffman, Nikos Tsagarakis

A Fail-Safe Semi-Centralized Impedance Controller: Validation on a Parallel Kinematics Ankle

Francesco Ruscelli[1,2], Arturo Laurenzi[1,2], Enrico Mingo Hoffman[1] and Nikos G. Tsagarakis[1]

***Abstract*— This paper proposes the implementation of an impedance controller on the ankle level of COMAN+, a robot with parallel kinematics ankles actuated by a dual four-bar mechanism. The main contribution of the work is a realization of said control scheme that grants a less abrupt and safer robot response in case of system failures, that would cause the local joint torque controllers to lose their torque reference inputs. In particular, we propose a semi-centralized impedance control implementation which eliminates the instability of the pure joint torque control schemes used in the classical fully centralized methods when torque reference interruptions occur. Finally, we present experimental results, proving the effectiveness of our method and demonstrating how it ensures a safer behaviour compared to a fully centralized impedance control implementation when the communication to the ankle joints is interrupted. This paper is a follow-up work of [1], which presented and analyzed the parallel kinematics ankles.**

I. Introduction

Robust locomotion of humanoid robots in complex environments is still an unsolved topic. Many solutions have been proposed, both on a higher behavioural level, e.g. footstep planning [2], [3] or balance recovery [4], and on a lower control level, such as active (admittance controller [5], [6], joint impedance control [7], Virtual Model Control [8]), and passive compliance (Series Elastic Actuators [9], [10], [11]). Furthermore, in implementing any control strategy particular emphasis should be put on the robot reliability: reducing, in the presence of communication interruptions between the centralized high layer controllers and the local actuation regulators, the risk of abrupt and unwanted reactions that could damage the robot and the environment or create unsafe conditions in human-robot interaction tasks. Similarly to the intrinsic elasticity of human muscles, which allows small adaptations to external obstacles and partial energy absorption from impacts [8], an effective solution to improve the interaction skills of robotics systems experiencing frequent dynamic interactions with the environment is the employment of impedance control schemes [12], [13]. Interacting effectively with the environment is very relevant to humanoids and in general to legged locomotion where the ability to conform and adapt to ground disturbances and impacts is a fundamental prerequisite for achieving stable locomotion. However, one of the limitations of the classical impedance control is its sensitivity to interruptions of torque reference signals for the local joint torque controllers. Due to the inherent instability of a pure joint torque regulator, if the communication between the centralized impedance control and the joint torque controllers is interrupted, unwanted torques are commanded to the motors. This could compromise the overall robot stability, creating dangerous situations for humans interacting with the robot and increasing the risk of damages both to the physical system and the environment.

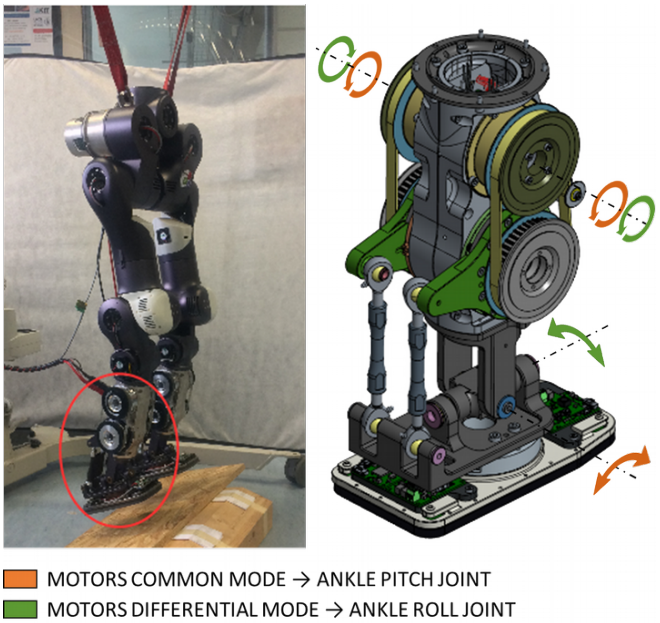

Fig. 1. The legs of the humanoid robot COMAN+ on the left and close back view of its tibia (CAD) without covers on the right. When the ankle's motors situated on the shin move in common mode (both rotate in the same direction, as illustrated by the orange arrows), a pitch motion is produced. Conversely, the motors moving in differential mode result in a roll motion of the ankle (green arrows).

In this work, we propose a method to realize a desired impedance using a partially centralized scheme that reduces abrupt motions when the torque reference of the actuators are interrupted. Specifically, our work is divided into two parts, both oriented towards the goal of devising an impedance controller capable of partially rejecting external perturbation while being more stable against interruptions in the actuation reference signals:

- the implementation of an impedance controller, on the humanoid COMAN+ (shown in Figure 1);
- the design of the Semi-Centralized Impedance Controller (SCIC), a specific formulation of the impedance controller based on a semi-centralized scheme.

The proposed control was implemented on the ankle joint,

[1]Department of Advanced Robotics, Istituto Italiano di Tecnologia (IIT), Via Morego 30, 16163 Genova
[2]DIBRIS, Università di Genova, Via Opera Pia 13, 16145, Italy
{francesco.ruscelli, arturo.laurenzi, enrico.mingo, nikos.tsagarakis}@iit.it

which is based on a parallel kinematics mechanism [1] and actuated by two motors through a dual four-bar transmission mechanism. Since the foot is the joint directly interacting with the terrain and hence subjected to impact forces and disturbances from the ground, compliant ankles could enhance the robot behaviour on uneven grounds, adapting its step to the terrain and rejecting minor disturbances on the joint.

The main motivation of this work is the realization and validation of the aforementioned controller so as to ensure the system stability and safety in the presence of failures, i.e. communication interruptions between the on-board centralized computer and actuation DSPs controllers. Such events could lead to unwanted torques commanded abruptly to the robot, leading to hardware damages or sudden motions, especially dangerous in human-robot interaction tasks. The Semi-Centralized Impedance Controller (SCIC) takes advantage of the local joint impedance controller implemented at each motor's DSP, sending the desired torque as two different components: the first depends only on the reference and the sensed position of the motor, while the second term is a bounded torque sent in feed-forward. This allows the robot, if the communication is interrupted, to keep the last motor position reference sent, while the feed-forward term becomes a bounded disturbance which is easily rejected.

Following the Introduction, in Section II we describe the transmission mechanism between joints and motors of the ankle. In Section III we present the impedance controller extended for the humanoid COMAN+. In Section IV we propose the semi-centralized impedance controller. Experimental results and relative discussion are presented in section V. Finally, conclusion and future works are discussed in section VI.

II. Joint-to-motor transmission

In this section, we describe the parallel ankle mechanism and the kinematics of the joint-motor transmission. A parallel ankle offers numerous advantages over its serial counterpart, though at the expense of more complex kinematics. By using a four-bar mechanism the motors of the ankle can be placed on the shin, decreasing the inertia of the tibia, improving the dynamic behaviour and reducing power consumption. Additionally, a parallel configuration allows the distribution of the torque provided by the actuators to the two degrees-of-freedom of each ankle: motors moving in common mode produce a pitch motion, while differential mode movement results in roll motion (see Figure 1). The transmission between the parallel ankle joint and actuators requires a transformation when passing from the motors variables to joint variables. In particular, joint and motor angles are related through a forward kinematic mapping, and differentiation yields the velocity mapping:

$$\dot{\mathbf{q}} = \mathbf{J}(\boldsymbol{\theta})\dot{\boldsymbol{\theta}}. \tag{1}$$

where $\mathbf{J}(\boldsymbol{\theta}) \in \mathbb{R}^{2\times 2}$ is the Jacobian for the parallel ankle mechanism of COMAN+, $\dot{\mathbf{q}} \in \mathbb{R}^2$ are the joint-side velocities and $\dot{\boldsymbol{\theta}} \in \mathbb{R}^2$ the motor-side velocities. A complete computation of the Jacobian for this mechanism can be found in [1]. From the principle of virtual work, we obtain a linear mapping between the motor and joint torques, which is required for the design of the ankle impedance controller:

$$\boldsymbol{\tau}_m = \mathbf{J}(\boldsymbol{\theta})^T \boldsymbol{\tau}_j, \tag{2}$$

where $\boldsymbol{\tau}_m \in \mathbb{R}^2$ is the torque sensed by the actuator and $\boldsymbol{\tau}_j \in \mathbb{R}^2$ is the torque at the joint (from now on we are going to drop the dependency on $\boldsymbol{\theta}$).

III. Impedance controller

In this section, we describe the implementation of an impedance controller on the parallel kinematics ankles of the humanoid robot COMAN+. The impedance controller at the motor-side has the following formulation:

$$\boldsymbol{\tau}_{m,d} = \mathbf{K}_m \Delta\boldsymbol{\theta} + \mathbf{D}_m \Delta\dot{\boldsymbol{\theta}} + \boldsymbol{\tau}_{m,\mathrm{ff}}, \tag{3}$$

where $\mathbf{K}_m \in \mathbb{R}^{2\times 2}$ and $\mathbf{D}_m \in \mathbb{R}^{2\times 2}$ are respectively the motor-side stiffness and the damping matrices, $\Delta\boldsymbol{\theta} = \boldsymbol{\theta}_d - \boldsymbol{\theta} \in \mathbb{R}^2$ is the error between the desired and measured motor positions, $\Delta\dot{\boldsymbol{\theta}} = \dot{\boldsymbol{\theta}}_d - \dot{\boldsymbol{\theta}} \in \mathbb{R}^2$ is the error between the desired and measured motor velocities and $\boldsymbol{\tau}_{m,\mathrm{ff}} \in \mathbb{R}^2$ are feed-forward reference torques at the motor-side. The same law can be defined at the ankle joint level:

$$\boldsymbol{\tau}_{j,d} = \mathbf{K}_j \Delta\mathbf{q} + \mathbf{D}_j \Delta\dot{\mathbf{q}} + \boldsymbol{\tau}_{j,\mathrm{ff}}, \tag{4}$$

where the quantities are defined w.r.t. the joint-side instead.

Our goal is to define a motor-side stiffness and damping matrix corresponding to a desired joint-side stiffness matrix:

$$\{\mathbf{K}_m, \mathbf{D}_m\} = \mathcal{T}\{\mathbf{K}_j, \mathbf{D}_j\}, \tag{5}$$

Since the ankle has two DoFs, pitch and roll, we design diagonal stiffness and damping matrices to decouple the effect of the impedance controller on the two axes:

$$\mathbf{K}_j = \begin{pmatrix} k_p & 0 \\ 0 & k_r \end{pmatrix}, \tag{6}$$

By using (2) and (3) we can write:

$$\begin{aligned} \mathbf{K}_m = \frac{\partial \boldsymbol{\tau}_m}{\partial \boldsymbol{\theta}} &= \frac{\partial (\mathbf{J}^T \mathbf{K}_j \Delta\mathbf{q})}{\partial \boldsymbol{\theta}} \\ &= \mathbf{J}^T \mathbf{K}_j \mathbf{J} + \cancelto{\mathbf{0}}{\frac{\partial \mathbf{J}^T}{\partial \boldsymbol{\theta}}} \mathbf{K}_j \Delta\mathbf{q}. \end{aligned} \tag{7}$$

It can be seen how this formulation is position dependent, since the mapping $\mathcal{T}$ changes with the robot configuration. If we compute the stiffness matrix around the equilibrium point ($\Delta\boldsymbol{\theta} = \mathbf{0}$) the second term $\frac{\partial \mathbf{J}^T}{\partial \boldsymbol{\theta}} \mathbf{K}_j \Delta\mathbf{q}$ can be discarded, though neglecting the conservativeness of the mapping: an in-depth analysis including this term is found in [14]. A similar approach can be used to obtain the damping $\mathbf{D}_j$:

$$\begin{aligned} \mathbf{D}_m = \frac{\partial \boldsymbol{\tau}_m}{\partial \dot{\boldsymbol{\theta}}} &= \frac{\partial (\mathbf{J}^T \mathbf{D}_j \Delta\dot{\mathbf{q}})}{\partial \dot{\boldsymbol{\theta}}} \\ &= \mathbf{J}^T \mathbf{D}_j \frac{\partial \dot{\mathbf{q}}}{\partial \dot{\boldsymbol{\theta}}} = \mathbf{J}^T \mathbf{D}_j \mathbf{J}, \end{aligned} \tag{8}$$

$$\mathbf{K}_j = \begin{pmatrix} k_p & 0 \\ 0 & k_r \end{pmatrix}, \qquad \mathbf{D}_j = \begin{pmatrix} d_p & 0 \\ 0 & d_r \end{pmatrix},$$
$$\mathbf{K}_m = \begin{pmatrix} k_a & k_c \\ k_c & k_b \end{pmatrix}, \qquad \mathbf{D}_m = \begin{pmatrix} d_a & d_c \\ d_c & d_b \end{pmatrix}. \tag{9}$$

In general, from a diagonal joint stiffness matrix $\mathbf{K}_j$, a non-diagonal motor stiffness matrix $\mathbf{K}_m$ is derived from the mapping. Finally, the term $\boldsymbol{\tau}_{m,\text{ff}}$ can be obtained from $\boldsymbol{\tau}_{j,\text{ff}}$ using (2).

It should be noted that $\frac{\partial(\mathbf{J}^T\mathbf{K}_j\Delta\mathbf{q})}{\partial\boldsymbol{\theta}} = \mathbf{J}^T\mathbf{K}_j\mathbf{J}$ is valid only locally [15], [14]. Therefore, large displacements from the equilibrium point lead to errors in the stiffness matrix. However, since the parallel ankle mechanism has a narrow range of motion, both on the pitch and the roll axes (i.e. the term $\Delta\mathbf{q}$ always remains relatively small), the mapping never causes significant errors.

Remark: In this paper, a traditional notation was used to describe the motor-joint mapping $\mathbf{q} = f(\boldsymbol{\theta})$ for the sake of clarity. However, in the robot we used the inverse mapping, since the kinematics were provided in this form by [1]. Following the calculations, we require the inverse of the Jacobian to obtain the motor torque: $\boldsymbol{\tau}_m = \mathbf{J}(\boldsymbol{\theta})^{-T}\boldsymbol{\tau}_j$. Thanks to the mechanical design of the ankle mechanism the matrix is square and has always full rank: therefore we don't run up against singularity issues.

IV. Semi-Centralized Impedance Control (SCIC)

In this section, we propose an implementation of an impedance controller to make the ankles less susceptible to hardware breakdown or disconnections, reducing potential movements that could compromise the hardware or create unsafe conditions in general. To achieve the desired behaviour in the ankle joint, the controller can be implemented in two different ways for a torque controlled robot.

Pure Torque Control. A conventional way is sending the computed torque directly to the torque controller implemented in each DSP. The on-board processor computes joint torques and transforms them into motor torques before sending them to the DSP of the actuator:

$$\boldsymbol{\tau}_{m,d} = \mathbf{J}^T\left(\mathbf{K}_j\Delta\mathbf{q} + \mathbf{D}_j\Delta\dot{\mathbf{q}} + \boldsymbol{\tau}_{j,\text{ff}}\right). \tag{10}$$

This method, although viable, is not robust against hardware failures that cause interruptions of the torque reference signals sent the joint local torque controllers. If the connection between the computer and the DSP is severed, the robot behaviour can become unstable, generating high speed motions that could damage the robot and the environment: having solely a torque reference and no position feedback, this impedance control implementation would directly send the last computed torque reference to the DSP causing the ankle to jolt against the mechanical limits with the risk of damaging the actuator transmission system or other mechanical components. Besides, such behaviour can severely compromise safety in any robotics application where humans are in close vicinity of the robot. Since most of the human-robot collaboration applications rely on the use of impedance control to generate compliant interactions, bounding the robot reactions in the case of system failures is critically necessary.

Semi-Centralized Impedance Control. A way to grant a safer response is sending to the DSP a position reference and the computed stiffness and damping diagonals, and let the DSP calculate the torque using the feedback of the robot. This allows to bound the system motion reaction, resulting in a graceful and safer degradation if a system failure causing discontinuities of the torque reference signals occurs.

To achieve this scheme, we can arrange the matrices $\mathbf{K}_m$ and $\mathbf{D}_m$, derived from the joint-motor transformation, in the following way:

$$\begin{aligned} \mathbf{K}_m &= \overline{\mathbf{K}}_m + \widetilde{\mathbf{K}}_m, \\ \mathbf{D}_m &= \overline{\mathbf{D}}_m + \widetilde{\mathbf{D}}_m, \end{aligned} \tag{11}$$

where $\overline{(\cdot)}_m$ contains the diagonal elements and $\widetilde{(\cdot)}_m$ contains the off-diagonal elements of the matrix. Recalling equation (3), we can write:

$$\boldsymbol{\tau}_{m,d} = \overline{\mathbf{K}}_m\Delta\boldsymbol{\theta} + \overline{\mathbf{D}}_m\Delta\dot{\boldsymbol{\theta}} + \boldsymbol{\tau}_{m,\text{ff}}, \tag{12}$$

where:

$$\boldsymbol{\tau}_{m,\text{ff}} = \widetilde{\mathbf{K}}_m\Delta\boldsymbol{\theta} + \widetilde{\mathbf{D}}_m\Delta\dot{\boldsymbol{\theta}} + \mathbf{J}^T\boldsymbol{\tau}_{j,\text{ff}}. \tag{13}$$

This formulation enables the decentralization of the input signals. The first two terms in (12) are computed in each DSP, each row separately. Conversely, the $\boldsymbol{\tau}_{m,\text{ff}}$ component in (13) is computed on the on-board computer in a centralized way: since the i^{th} DSP has information solely about the i^{th} actuator to which is connected, it can only determine the torques dependent on position θ_i and velocity $\dot{\theta}_i$, whereas both terms (θ_i and $\dot{\theta}_i$, $\forall i = 1, 2$) are needed to obtain each motor total torque. Therefore, the on-board computer uses the off-diagonal terms $\widetilde{\mathbf{K}}_m$ and $\widetilde{\mathbf{D}}_m$ to compute the part of the torque that depends on the other joint, which is then sent directly to the DSP as a feed-forward component. Term $\boldsymbol{\tau}_{j,\text{ff}}$ is a torque directly commanded to the joint by the user. Thus, in case of a failure:

- the last position sent to the robot is tracked by the DSP which continuously receive the position feedback locally;
- the last feed-forward torques received, provided by the remaining components of the stiffness and damping matrices, will act as a disturbance in the resultant position feedback loop implemented using the diagonal stiffness and damping elements. However, this disturbance is always bounded and not large enough to induce instabilities.

Our controller, in case of system faults that could interrupt the references signals to the joint local controllers, is then reduced to a simple closed loop with a bounded disturbance at the input which can be rejected. This favors the hardware protection and results in slower and safer robot reactions, especially important in human-robot interaction.

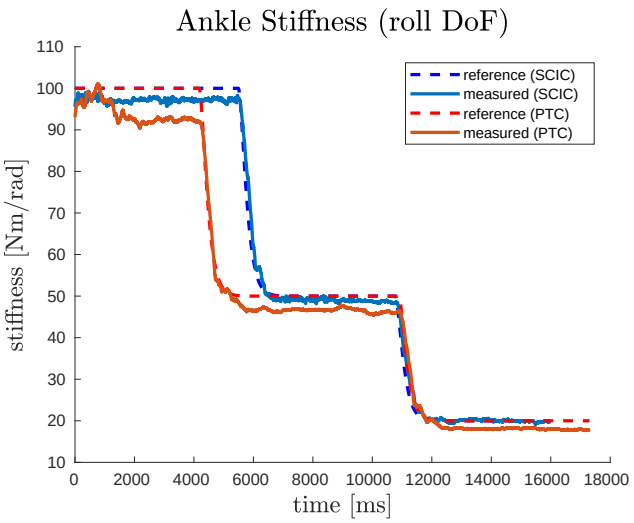

Fig. 2. Reference stiffness for the roll axis DoF commanded manually by the user (steps of 100, 50, 20 Nm/rad) compared to the measured ankle stiffness with the semi-centralized impedance control (SCIC) and the pure torque control (PTC).

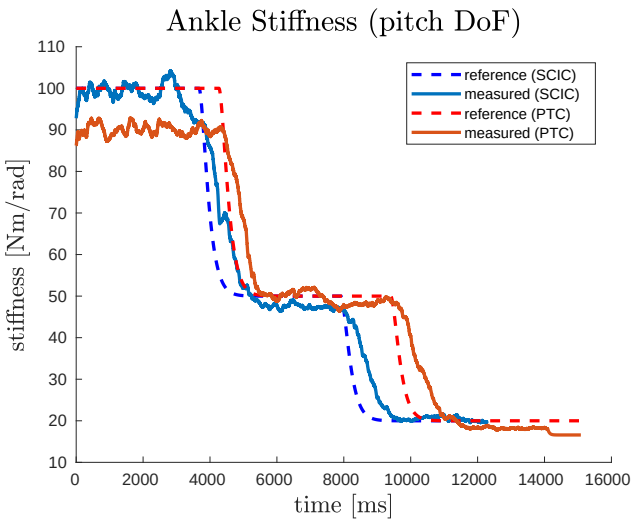

Fig. 3. Reference stiffness for the pitch axis DoF commanded manually by the user (steps of 100, 50, 20 Nm/rad) compared to the measured ankle stiffness with the semi-centralized impedance control (SCIC) and the pure torque control (PTC).

Remark: A similar semi-centralized method was implemented in [14] under different circumstances, i.e. a Cartesian impedance controller used to implement a compliant behaviour for robotic manipulators. However, the rationale behind our implementation differs from the one in [14], as we are exploiting it to demonstrate its benefits in ensuring a bounded robot reaction in case of system failures.

V. Experiments and Discussion

The robot platform used in this work is the lower body of the humanoid robot COMAN+, built at IIT, composed of 13 series elastic actuated (SEA) joints, providing a first layer of passive compliance and the ability to sense external forces. The software architecture of COMAN+ is powered by XBotCore [16], a software framework which permits to run hard real-time control loops at 1 kHz. The ankles motors were controlled in impedance mode: the control loop in each DSP consists of an impedance controller which takes as inputs the desired torque together with desired values of stiffness and damping. The impedance controller sends the computed reference torque to the lower-level torque controller of the actuator.

To validate the SCIC we compared it to the conventional pure torque control (PTC). In particular, we designed two classes of experiments to estimate performance, detailed in V-A and V-B: the first one is a set of experiments to measure the accuracy of the SCIC in rendering a desired impedance, and the second is a qualitative comparison to prove its efficacy in reducing the system motion reaction when a failure occurs. Finally, an experiment was designed to show qualitatively the advantages of an impedance controller implemented on the ankle joint. While lifted by the crane, the robot was set in a fixed standing configuration. Subsequently, it was lowered on an inclined wooden board. The experiment was repeated using three different strategies on the ankle joint:

- impedance control mode;
- position control mode;
- no control.

Videos of the experimental comparisons can be found at `https://youtu.be/-QULP4xUD9A`.

A. Accuracy validation

For the sake of clarity, we conducted two independent set of experiment, one for the stiffness alone and one for the damping, so that we could decouple the effects of damping and stiffness in (4). The feed-forward commanded torque was set to zero. Separate experiments were carried out for both ankle DoFs. The robot was lifted with a crane in order to raise it above the ground, starting with a nominal commanded stiffness (or damping). Then, an external force was applied along one DoF of the left ankle, while the commanded stiffness (or damping) was changed by the user. In particular, the ankle was kept in place while changing the stiffness reference, since its value depends on the position error. On the contrary, the damping depends on the velocity error; hence the ankle was moved while changing the damping reference to estimate its value. The sensed motor torque and position were translated into the sensed joint torque and position by using the Jacobian associated with the joint-motor mapping. A simple way to obtain the measured stiffness (or damping) is rearranging (4), but the results are way too noisy. Hence, we used a Recursive Least Square Filter (RLSF) to estimate the desired values. This adaptive algorithm allows to recursively evaluate stiffness and damping over time by minimizing a weighted least square cost function. We conducted two experiments for each degree of freedom, one for the stiffness and one for the damping.

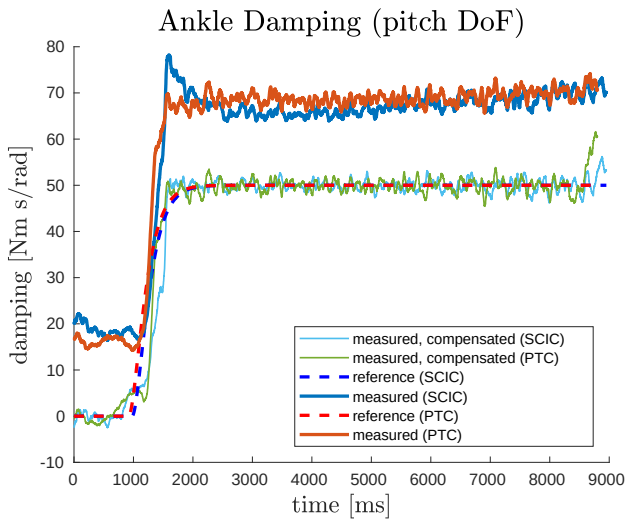

Fig. 4. Reference damping for the pitch axis DoF commanded manually by the user (one step from 0 to 50 Nm s/rad) compared to the measured ankle damping with the semi-centralized impedance control (SCIC) and the pure torque control (PTC). The offset between measured and reference values is due to a torque tracking error. The compensated measures are shown, closely tracking the reference values of damping.

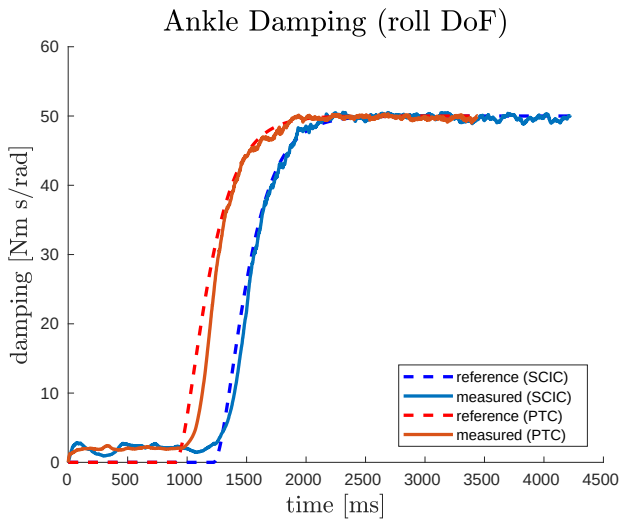

Fig. 5. Reference damping for the roll axis DoF commanded manually by the user (one step from 0 to 50 Nm s/rad) compared to the measured ankle damping with the semi-centralized impedance control (SCIC) and the pure torque control (PTC).

B. *Efficacy validation*

To validate our controller compared to the traditional one in the case of communication interruptions, we used the same experimental setting of the previous experiments, keeping the robot above the ground. While the SCIC was controlling the ankle with a non-zero stiffness and damping, a force was applied along one axis. In this configuration, the EtherCAT cable connecting the on-board computer to the actuators was unplugged, simulating a hardware failure. The same experiment was conducted with a pure torque input controller.

C. *Results*

The first class of experiments validated the accuracy of our method compared to the traditional torque input approach. Figures 2 and 3 shows the reference stiffness signal and the measured stiffness using the semi-centralized impedance controller (SCIC) and a pure torque input (PTC) for the roll and pitch DoF, respectively. Figures 4 and 5 shows the same graphs for the measured damping. All the measured values are filtered with the Recursive Least Square (RLS) filter. Note that the differences between the two reference values in each graph are due to the fact that the data for the SCIC and for the PTC belongs to separate experiments and the commands sent to the robot by the user differ in time. The measures from the SCIC are close to the reference signal and comparable to the ones from the PTC, thus validating our method.

The second experiment demonstrates the effectiveness of the SCIC's design: as the disconnection between on-board computer and DSPs occurs, our approach allows the ankle's DSP to keep the last position sent by the SCIC, while using the traditional control the last torque sent before the disconnection is kept as reference input, resulting in a rapid motion of the ankle joint towards its limit. Figure 7 shows a sequence of frames comparing the behaviour of the robot controlled with the SCIC and the PTC. Due to the nature of this particular experiment, i.e. unplugging the etherCAT cable to simulate a hardware failure, we couldn't collect any data.

Finally, the qualitative experiment proved the importance of the impedance control in granting the robot ankles with the ability to conform to the terrain. The ankles adapt to the slope without yielding under the weight of the robot. This desired behaviour falls between two unwanted extremes, shown in the remaining trials of Figure 8: the stiff position control doesn't allow the ankle to comply with the terrain, which rigidly keeps its position when the robot is lowered on the inclined board, while a non-controlled ankle collapses under the weight of the robot. Note that in these experiments we don't implement any balancing strategy on the robot, which is standing entirely thanks to its initial configuration.

A video including the full sequence of the controllers comparison (SCIC-PTC) and the qualitative experiments is available at `https://youtu.be/-QULP4xUD9A`.

D. *Offset discussion*

In this section, we discuss the offset between the reference signal and the measured values in the graphs of Figures 2, 3, 5 and 4. The offset error, which is particularly evident in Figure 4, arises from an offset in the torque tracking of the motor lower level control, which is shown in Figure 6. The corresponding stiffness and damping offset can be computed by solving the equation (4) for the stiffness or the damping. Note that the equation always has one addend only, since in the experiments either pure stiffness or damping was commanded to the robot and the feed-forward component was set to zero. The following expression is obtained for the stiffness offset:

$$\delta \boldsymbol{K}_j^{\text{meas}} = \text{diag}\left(\Delta \mathbf{q}\right)^{-1} \mathbf{J}^{-T} \cdot \delta \boldsymbol{\tau}_j^{\text{meas}} \qquad (14)$$

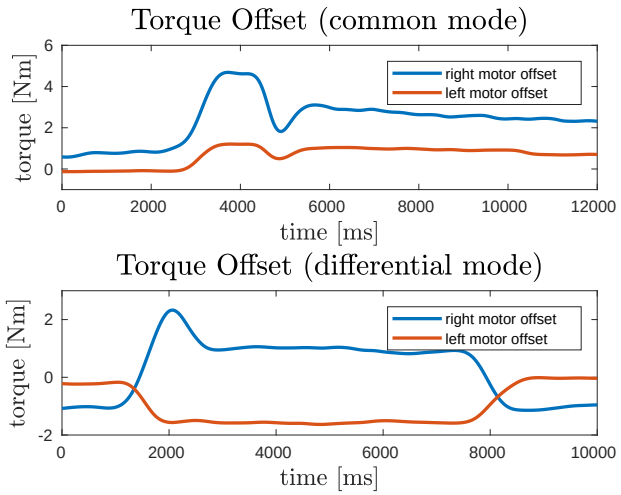

Fig. 6. Torque offset caused by a torque tracking error of the motor lower level control, filtered with a zero-phase digital filter. Above: the ankle motors are moving in common mode, resulting in a rotation of the ankle along the pitch axis. The torque offsets have the same sign. Below: the ankle motors are moving in differential mode, resulting in a rotation of the ankle along the roll axis. The torque offsets have opposite sign.

where $\delta \boldsymbol{K}_j^{\text{meas}}$ and $\delta \boldsymbol{\tau}_j^{\text{meas}}$ are the offset error in the measured stiffness and torque, respectively. Since we measure the torque on the motor level, we use equation (2) to map the sensed torque to the joint level and compute $\delta \boldsymbol{\tau}_j^{\text{meas}}$.

A similar equation can be written to estimate the offset in the damping:

$$\delta \boldsymbol{D}_j^{\text{meas}} = \text{diag}\left(\Delta \dot{\mathbf{q}}\right)^{-1} \mathbf{J}^{-T} \cdot \delta \boldsymbol{\tau}_j^{\text{meas}} \tag{15}$$

Both experiments to estimate stiffness and damping have an offset, but in the stiffness experiments the error is significantly smaller. This is due to the different nature of the two experiments: since the quality of the torque tracking is worse during torque reference variations, the experiment to estimate the damping, in which the ankle is moved, is affected by a higher torque tracking error compared to the experiment to estimate the stiffness, in which the ankle stays still. In the first graph of Figure 6 the two motors actuating the ankle joint are moving in common mode, and their offsets are concordant. In the second graph the two motors are moving in differential mode, and their offsets are discordant. This justifies both the offset in Figure 4, where the offsets from the two motor readings sum up, as well as the absence of an error in Figure 5, where the two errors cancel each other out. Finally, Figure 4 shows the damping measures corrected by compensating the offset: the resulting values follow closely the reference signal.

VI. Conclusion

The semi-centralized impedance controller was successfully implemented on the COMAN+ robot, extending it for the parallel kinematics mechanism of the ankles. We experimentally proved the effectiveness of our method, which performs closely to a conventional impedance control implementation based on pure local torque controllers: no evident difference is present between the experimental data of the SCIC and the PTC, as shown in Figures 2 - 5. The

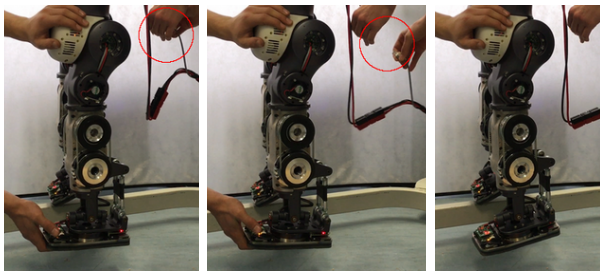

(a) The SCIC allows a safe response of the robot when the external force exerted on the robot is removed, the robot tracks the last position sent by the controller, returning to the nominal configuration.

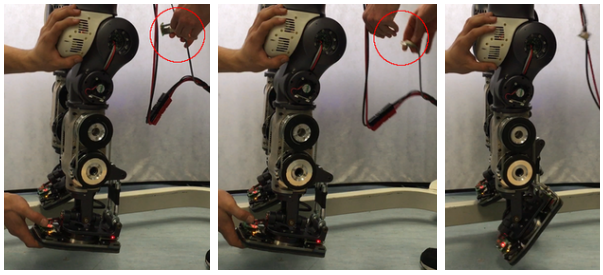

(b) The PTC makes the ankle jolt, reaching violently the joint limit, when the external force exerted on the robot is removed. This sudden reaction could push the robot off balance or cause damages to the ankle joint.

Fig. 7. Sequence of frames of the robot COMAN+'s behaviour when disconnected from the on-board computer. The red circles highlight the etherCAT, which is unplugged in the second frame simulating a hardware failure.

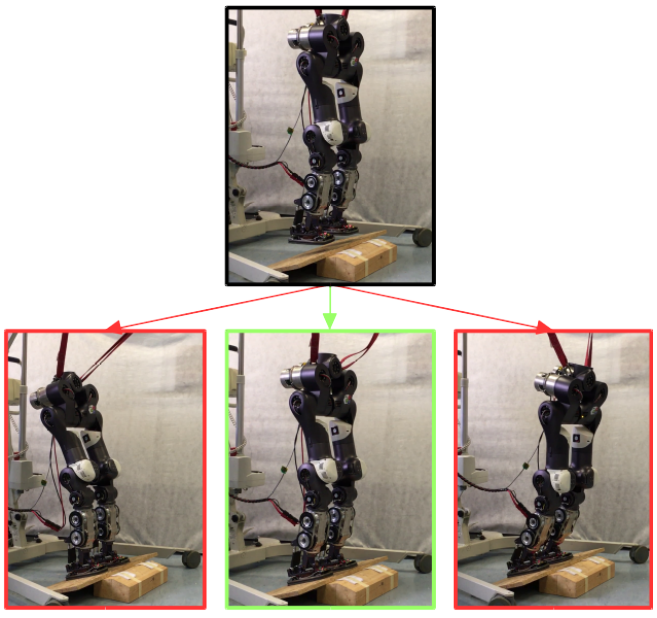

Fig. 8. Frames of the COMAN+ robot being lowered on a wooden board inclined of 16°. In a) the robot is position-controlled. The ankles don't adapt to the slope, making the robot fall backward. In b) the robot is controlled with an impedance controller (stiffness: 30 Nm/rad, damping: 5 Nm s/rad), which allows the ankles to comply with the inclined board. Finally, in c) the robot is not controlled. The ankles collapse under the weight of the robot, making it fall forward.

offset error in the measurements, due to the torque tracking error in the lower control, was analyzed and effectively compensated. Furthermore, we showed how the implementation of the impedance controller improves the behaviour of the COMAN+ lower body, allowing the ankles to comply with the environment.

The main contribution of this paper is the design, implementation and testing of an impedance controller capable of withstanding potential system failures without generating rapid motion reactions, which could compromise the hardware integrity or the safety of humans interacting with the robot. This is a fundamental prerequisite for a robotic platform used in real-time operations such as human-robot interactions or rescue missions, where the effects of failure should be reduced as much as possible to protect both the hardware and the human operators. Our implementation allows the robot to fail gracefully, as opposed to a traditional impedance control implementation relying on pure local torque controllers, in which interruptions or breakdowns of the main on-board computer could lead to abrupt movements of the joints and dangerous behaviours. The SCIC was experimentally validated in the presence of disconnections: by simulating a hardware failure, we proved how the ankle doesn't drift violently, but returns to its nominal position. This paper follows the development of the new robot COMAN+: future work will build upon this work to further develop and apply the proposed scheme to the full humanoid robot.

ACKNOWLEDGEMENTS

The research leading to these results has received funding from the European Union Horizon 2020 robotics program [ICT-23-2014], grant agreements n.644727 (CogIMon).

REFERENCES

[1] C. Zhou and N. Tsagarakis, "On the Comprehensive Kinematics Analysis of a Humanoid Parallel Ankle Mechanism," *ASME Journal of Mechanisms and Robotics, under review*, 2018.

[2] A. Herdt, H. Diedam, P.-B. Wieber, D. Dimitrov, K. Mombaur, and M. Diehl, "Online Walking Motion Generation with Automatic Footstep Placement," *Advanced Robotics*, vol. 24, no. 5-6, pp. 719–737, jan 2010.

[3] J. E. Chestnutt, M. Lau, G. K. M. Cheung, J. Kuffner, J. K. Hodgins, and T. Kanade, "Footstep Planning for the Honda ASIMO Humanoid." in *IEEE International Conference on Robotics and Automation (ICRA)*, 2005, pp. 629–634.

[4] B. Stephens, "Humanoid push recovery," in *IEEE/RAS International Conference on Humanoid Robots (HUMANOIDS)*, 2007, pp. 589–595.

[5] C. Zhou, Z. Li, J. Castano, H. Dallali, N. G. Tsagarakis, and D. G. Caldwell, "A passivity based compliance stabilizer for humanoid robots," *IEEE International Conference on Robotics and Automation (ICRA)*, pp. 1487–1492, 2014.

[6] Z. Li, N. Tsagarakis, and D. G. Caldwell, "A Passivity Based Admittance Control for Stabilizing the Compliant Humanoid COMAN," in *IEEE/RAS International Conference on Humanoid Robots (HUMANOIDS)*, Osaka, Japan, 2012.

[7] E. Mingo Hoffman, N. Perrin, N. G. Tsagarakis, and D. G. Caldwell, "Upper limb compliant strategy exploiting external physical constraints for humanoid fall avoidance," in *IEEE/RAS International Conference on Humanoid Robots (HUMANOIDS)*, 2013, pp. 397–402.

[8] J. E. Pratt, C.-M. Chew, A. Torres, P. Dilworth, and G. A. Pratt, "Virtual Model Control: An Intuitive Approach for Bipedal Locomotion." *I. J. Robotic Res.*, vol. 20, no. 2, pp. 129–143, 2001.

[9] G. Pratt and M. Williamson, "Series elastic actuators," in *IEEE/RSJ International Conference on Intelligent Robots and Systems (IROS)*, vol. 1, 1995, pp. 399–406.

[10] N. G. Tsagarakis, S. Morfey, G. Medrano Cerda, L. Zhibin, and D. G. Caldwell, "COMpliant huMANoid COMAN: Optimal joint stiffness tuning for modal frequency control," in *IEEE International Conference on Robotics and Automation (ICRA)*, may 2013, pp. 673–678.

[11] N. G. Tsagarakis, D. G. Caldwell, F. Negrello, W. Choi, L. Baccelliere, V. Loc, J. Noorden, L. Muratore, A. Margan, A. Cardellino, L. Natale, E. Mingo Hoffman, H. Dallali, N. Kashiri, J. Malzahn, J. Lee, P. Kryczka, D. Kanoulas, M. Garabini, M. Catalano, M. Ferrati, V. Varricchio, L. Pallottino, C. Pavan, A. Bicchi, A. Settimi, A. Rocchi, and A. Ajoudani, "WALK-MAN: A High-Performance Humanoid Platform for Realistic Environments," *Journal of Field Robotics*, vol. 34, no. 7, pp. 1225–1259, oct 2017.

[12] Jong Hyeon Park and Hoam Chung, "Hybrid control for biped robots using impedance control and computed-torque control," in *IEEE International Conference on Robotics and Automation (ICRA)*, vol. 2, 1999, pp. 1365–1370.

[13] Hun-ok Lim, S. Setiawan, and A. Takanishi, "Balance and impedance control for biped humanoid robot locomotion," in *IEEE/RSJ International Conference on Intelligent Robots and Systems (IROS).*, vol. 1, 2001, pp. 494–499.

[14] A. Albu-Schäffer and G. Hirzinger, "Cartesian impedance control techniques for torque controlled light-weight robots," in *IEEE International Conference on Robotics and Automation (ICRA)*, vol. 1, 2002, pp. 657–663.

[15] A. Albu-Schäffer, M. Fischer, G. Schreiber, F. Schoeppe, and G. Hirzinger, "Soft robotics: what cartesian stiffness can obtain with passively compliant, uncoupled joints?" in *IEEE/RSJ International Conference on Intelligent Robots and Systems, (IROS).*, vol. 4. IEEE, 2004, pp. 3295–3301.

[16] L. Muratore, A. Laurenzi, E. M. Hoffman, A. Rocchi, D. G. Caldwell, and N. G. Tsagarakis, "XBotCore: A Real-Time Cross-Robot Software Platform," in *First IEEE International Conference on Robotic Computing (IRC)*. IEEE, apr 2017, pp. 77–80.